Order online now!

www.rockland.com
tech@rockland.com
+1 484.791.3823

Datasheet for 600-401-384

HA Epitope Tag Antibody

Overview

Description:	Anti-HA Epitope Tag (RABBIT) Antibody - 600-401-384
Item No.:	600-401-384
Size:	100 µg
Applications:	ELISA, IHC, WB, IF, IP, Multiplex
Reactivity:	HA-Tag
Host Species:	Rabbit

Product Details

Background:	Epitope tags are short peptide sequences that are easily recognized by tag-specific antibodies. Due to their small size, epitope tags do not affect the biochemical properties of the tagged protein. Most often, sequences encoding the epitope tag are included with the target DNA at the time of cloning to produce fusion proteins containing the epitope tag sequence. This allows Anti epitope tag antibodies to serve as universal detection reagents for any tag containing protein produced by recombinant means. This means that anti-epitope tag antibodies are a useful alternative to generating specific antibodies to identify, immunoprecipitate or immunoaffinity purify a recombinant protein. HA tag is frequently incorporated into recombinant proteins for a variety of purposes. An anti-HA antibody can then be used to detect the protein when doing studies with transfected cells.
Synonyms:	rabbit anti-HA epitope tag antibody, rabbit anti-hemagglutinin antibody, rabbit anti-HA tag antibody, anti-epitope
Host Species:	Rabbit
Clonality:	Polyclonal
Format:	IgG

Target Details

Reactivity:	HA-Tag
Immunogen Type:	Conjugated Peptide

Immunogen:	Anti-HA antibody was purified from whole rabbit serum prepared by repeated immunizations with the epitope tag peptide YPYDVPDYA (114-122) from hemagglutinin influenza conjugated to KLH.
Purity/Specificity:	This affinity purified Anti-HA antibody is directed against the HA motif and is useful in determining its presence in various assays. This polyclonal anti-HA tag antibody detects over-expressed proteins containing the HA epitope tag. To date, this antibody has reacted with all HA-tagged proteins tested. In western blotting of bacterial extracts, the antibody does not cross-react with endogenous proteins.

Application Details

Tested Applications:	ELISA, IHC, WB
Suggested Applications:	IF, IP, Multiplex (Based on references)
Application Note:	Anti-HA is optimally suited for monitoring the expression of HA-tagged fusion proteins. As such, anti-HA/HA can be used to identify fusion proteins containing the HA epitope. The antibody recognizes the HA epitope tag fused to the amino- or carboxy- termini of targeted proteins, as expressed in many commonly used expression vectors. This antibody has been tested by ELISA, immunohistochemistry, and western blotting against both the immunizing peptide and HA containing recombinant proteins. Although not tested, this antibody is likely functional for immunoprecipitation, immunocytochemistry, and other immunodetection techniques. Affinity purification of the polyclonal antibody results in very low background levels in assays and low cross-reactivity with other cellular proteins.
Assay Dilutions:	All assays should be optimized by the user. Recommended dilutions (if any) may be listed below.
ChIP:	User Optimized
ELISA:	1:10,000 - 1:100,000
IHC:	1:500 - 1:2,000
IP:	User Optimized
WB:	1:2,000 - 1:10,000

Formulation

Physical State:	Liquid (sterile filtered)
Concentration:	1.05 mg/mL by UV absorbance at 280 nm
Buffer:	0.02 M Potassium Phosphate, 0.15 M Sodium Chloride, pH 7.2
Preservative:	0.01% (w/v) Sodium Azide
Stabilizer:	None

Shipping & Handling

Shipping Condition:	Dry Ice
Storage Condition:	Store vial at -20° C prior to opening. Aliquot contents and freeze at -20° C or below for extended storage. Avoid cycles of freezing and thawing. Centrifuge product if not completely clear after standing at room temperature. This product is stable for several weeks at 4° C as an undiluted liquid. Dilute only prior to immediate use.
Expiration:	Expiration date is one (1) year from date of receipt.

Images

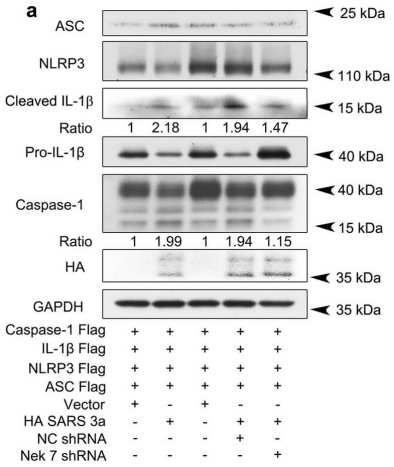

Western Blot
SARS 3a induces NLRP3 inflammasome activation by multiple mechanisms. A) Immunoblot analysis of the pro- and cleaved forms of caspase-1 and IL-1β after reconstitution of inflammasome in HEK 293T cells transfected with SARS 3a with or without NEK7 shRNA. B) Immunoblot analysis of the pro- and cleaved forms of caspase-1 and IL-1β after reconstitution of inflammasome and transfection with SARS 3a or SARS 3a C133A. C) Immunoblot analysis of the pro- and cleaved forms of caspase-1 and IL-1β after co-transfection with caspase-1, IL-1β, and SARS 3a or SARS 3a C133A. d Immunoprecipitation analysis of interaction between SARS 3a or SARS 3a C133A and caspase-1. All western blot data are representative of two or three independent experiments Figure provided by CiteAb. Source: Cell Death Dis, PMID: 30185776.

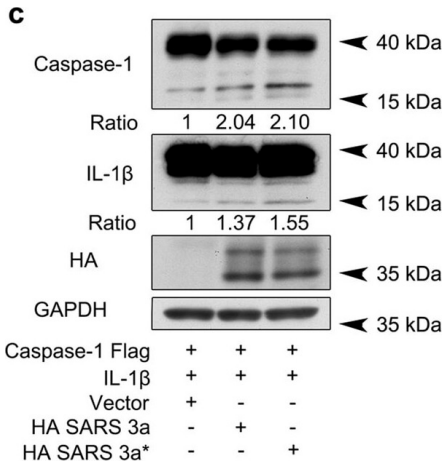

Western Blot

SARS 3a induces NLRP3 inflammasome activation by multiple mechanisms. A) Immunoblot analysis of the pro- and cleaved forms of caspase-1 and IL-1β after reconstitution of inflammasome in HEK 293T cells transfected with SARS 3a with or without NEK7 shRNA. B) Immunoblot analysis of the pro- and cleaved forms of caspase-1 and IL-1β after reconstitution of inflammasome and transfection with SARS 3a or SARS 3a C133A. C) Immunoblot analysis of the pro- and cleaved forms of caspase-1 and IL-1β after co-transfection with caspase-1, IL-1β, and SARS 3a or SARS 3a C133A. D) Immunoprecipitation analysis of interaction between SARS 3a or SARS 3a C133A and caspase-1. All western blot data are representative of two or three independent experiments Figure provided by CiteAb. Source: Cell Death Dis, PMID: 30185776.

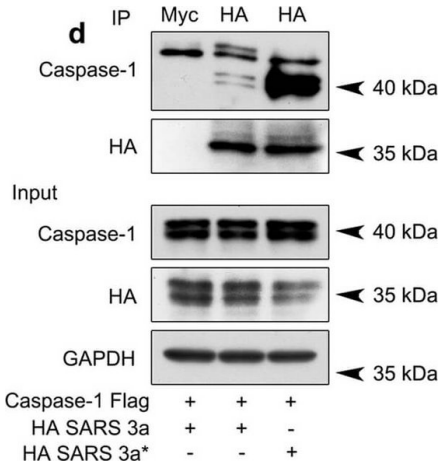

Western Blot

SARS 3a induces NLRP3 inflammasome activation by multiple mechanisms. A) Immunoblot analysis of the pro- and cleaved forms of caspase-1 and IL-1β after reconstitution of inflammasome in HEK 293T cells transfected with SARS 3a with or without NEK7 shRNA. B) Immunoblot analysis of the pro- and cleaved forms of caspase-1 and IL-1β after reconstitution of inflammasome and transfection with SARS 3a or SARS 3a C133A. C) Immunoblot analysis of the pro- and cleaved forms of caspase-1 and IL-1β after co-transfection with caspase-1, IL-1β, and SARS 3a or SARS 3a C133A. D) Immunoprecipitation analysis of interaction between SARS 3a or SARS 3a C133A and caspase-1. All western blot data are representative of two or three independent experiments Figure provided by CiteAb. Source: Cell Death Dis, PMID: 30185776.

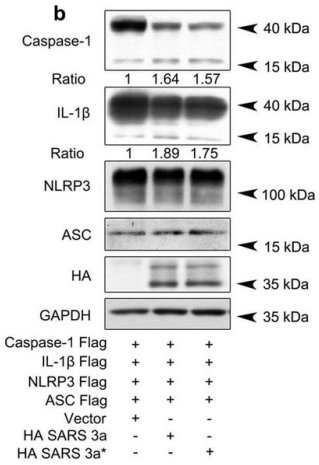

Western Blot

SARS 3a induces NLRP3 inflammasome activation by multiple mechanisms. A) Immunoblot analysis of the pro- and cleaved forms of caspase-1 and IL-1β after reconstitution of inflammasome in HEK 293T cells transfected with SARS 3a with or without NEK7 shRNA. B) Immunoblot analysis of the pro- and cleaved forms of caspase-1 and IL-1β after reconstitution of inflammasome and transfection with SARS 3a or SARS 3a C133A. C) Immunoblot analysis of the pro- and cleaved forms of caspase-1 and IL-1β after co-transfection with caspase-1, IL-1β, and SARS 3a or SARS 3a C133A. D) Immunoprecipitation analysis of interaction between SARS 3a or SARS 3a C133A and caspase-1. All western blot data are representative of two or three independent experiments Figure provided by CiteAb. Source: Cell Death Dis, PMID: 30185776.

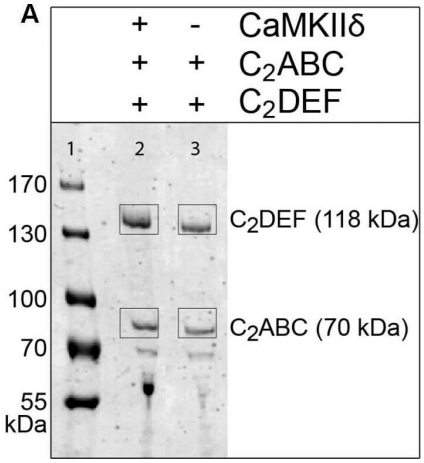

Western Blot

Otoferlin is phosphorylated by CaMKIIδ in vitro. (A) Otoferlin fragments C2ABC (aa 1–616 in NP_001093865, 70 kDa) and C2DEF (aa 908–1932, 118 kDa), were expressed in E. coli and subjected to an in vitro phosphorylation assay with CaMKIIδ and Ca2+/calmodulin. Reactions were stopped after 5 min of incubation and proteins were run on a Coomassie gel. Note the slight shift in mass of the fragments between experiment (lane 2) and control without kinase (lane 3). Coomassie stained bands corresponding to otoferlin C2DEF and C2ABC were cut off the gel and processed for mass spectrometric analysis of otoferlin phosphorylation (Supplementary Figure S2). (B) Three independent experiments as in (A) revealed 10 serine/threonines in otoferlin that were reproducibly phosphorylated by CaMKIIδ. The putative otoferlin domain topology (in mouse isoform 1; NP_001093865) predicts six C2 domains (C2A to C2F; purple), a coiled-coiled domain (orange), a FerB domain (yellow), and a transmembrane domain (TM) (dark gray). Five of the phosphorylation sites are located in C2 domains. Figure provided by CiteAb. Source: Front Synaptic Neurosci, Figure 6. PMID: 29046633.

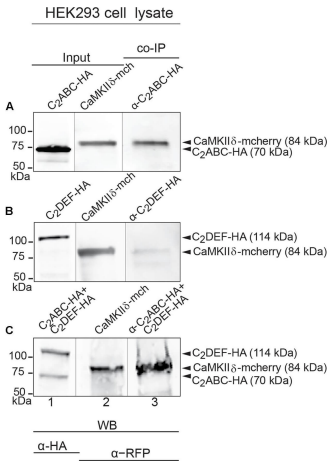

Western Blot

Immunoprecipitation and western blot show interaction of otoferlin with CaMKIIδ. (A–C) Two HA-tagged mouse otoferlin fragments, C2ABC (aa 1–632 in NP_001093865; 70 kDa) and C2DEF (aa 933–1920; 114 kDa) were co-transfected with mcherry-tagged mouse CaMKIIδ into HEK293 cells. Transfections were performed either with otoferlin C2ABC and CaMKIIδ (A, Input Lane 1 and 2), otoferlin C2DEF and CaMKIIδ (B, Input Lane 1 and 2) or in the presence of both C2ABC and C2DEF fragments and CaMKIIδ (C, Input Lane 1 and 2). Co-immunoprecipitations of C2ABC-HA and C2DEF-HA were conducted from HEK293 cell lysates using anti-HA antibodies. CaMKIIδ-mcherry was detected in the eluate using an anti-RFP (red fluorescent protein) antibody (A–C, Lane 3), indicating that CaMKIIδ co-precipitated with recombinant otoferlin fragments. Figure provided by CiteAb. Source: Front Synaptic Neurosci, PMID: 29046633.

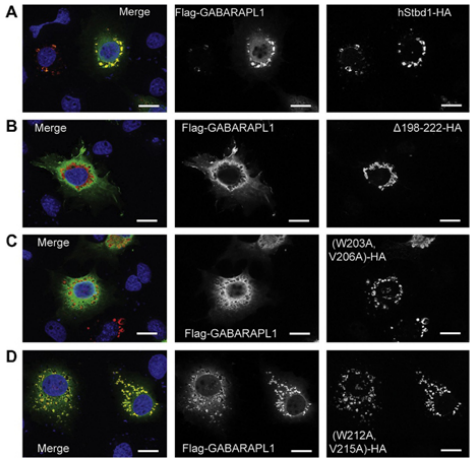

Immunofluorescence Microscopy

Subcellular localization of GABARAPL1 and Atg8 family interacting motif (AIM) mutants of Stbd1 co-expressed in COS M9 cells. Mutated hStbd1 with a C-terminal HA-tag was co-expressed in COS M9 cells with N-terminal Flag-tagged GABARAPL1 and immunostained with anti-HA antibodies (red) or anti-Flag antibodies (green). (A) Co-localization of hStbd1 and GABARAPL1 (merged in left panel) in cells co-expressing C-terminal HA-tagged full length hStbd1 (right panel) and N-terminal Flag-tagged GABARAPL1 (middle panel). (B) Loss of co-localization (merged in left panel) of Flag-tagged GABARAPL1 (middle panel) with potential AIM deletion mutant of hStbd1, Δ198–222–HA (right panel). (C) Impaired co-localization (merged in left panel) of Flag-tagged GABARAPL1 (middle panel) with double mutation in a potential AIM on hStbd1, (W203A, V206A)-HA (right panel). (D) Unaffected co-localization (merged in left panel) of Flag-tagged GABARAPL1 (middle panel) with double mutation in another potential AIM on hStbd1, (W212A, V215A)-HA (right panel). Nuclei were stained with Hoechst (blue). The scale bar is 20 µm. Fig 3. PMID: 21893048

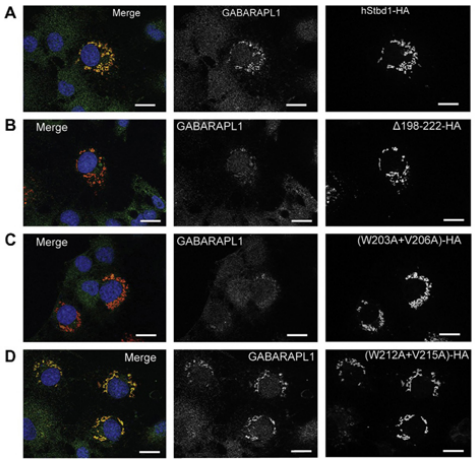

Immunofluorescence Microscopy
Subcellular localization of endogenous GABARAPL1 and overexpressed Stbd1 with Atg8 family interacting motif (AIM) mutations in COS M9 cells. Overexpressed full length or mutated hStbd1 with a C-terminal HA-tag and endogenous GABARAPL1 in COS M9 cells was immunostained with anti-HA antibodies (red) or anti-GABARAPL1 antibodies (green). (A) Co-localization of hStbd1 and GABARAPL1 (merged in left panel) in cells expressing C-terminal HA-tagged full length hStbd1 (right panel) and endogenous GABARAPL1 (middle panel). (B) Loss of co-localization (merged in left panel) of endogenous GABARAPL1 (middle panel) with potential AIM deletion mutant of hStbd1, Δ198–222–HA (right panel). (C) Impaired co-localization (merged in left panel) of endogenous GABARAPL1 (middle panel) with double mutation in potential AIM on hStbd1, (W203A, V206A)-HA (right panel). (D) Unaffected co-localization (merged in left panel) of endogenous GABARAPL1 (middle panel) with double mutation in another potential AIM on hStbd1, (W212A, V215A)-HA (right panel). Nuclei were stained with Hoechst (blue). The scale bar is 20 µm. Fig 4. PMID: 21893048

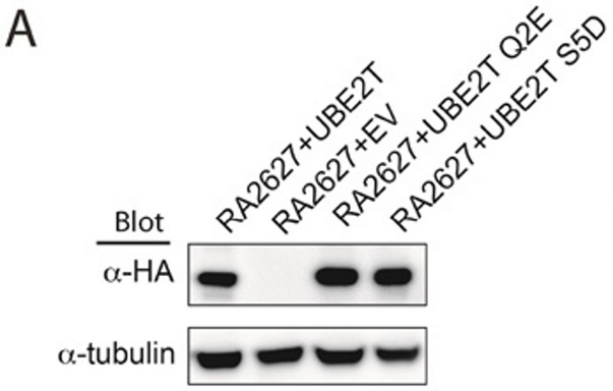

Western Blot
hUBE2T-deficient RA2627 cells expressing hUBE2T S5D phosphomimetic are defective for FANCD2 and FANCI monoubiquitination. (A) Anti-HA western blot of hUBE2T deficient transformed and immortalized RA2627 E6/E7/hTERT fibroblasts expressing the indicated protein. Figure 7. PMID: 28162934

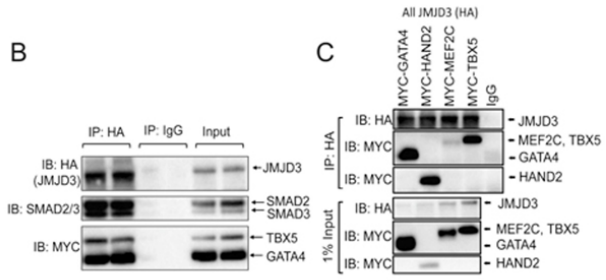

Western Blot

B) Co-IPs using nuclear lysates harvested from HEK293T cells transfected with MYC-GHMT and HA-JMJD3. Following Co-IP with anti-HA, proteins were resolved by SDS-PAGE and immunoblotted for MYC, HA, and SMAD2/3. C) Co-IPs using nuclear lysates harvested from HEK293T cells transfected with HA-JMJD3 and individual MYC-G, -H, –M, or -T transcription factors. Following Co-IP with anti-HA (C), proteins were resolved by SDS-PAGE and immunoblotted for HA. Fig 2. PMID: 33359755

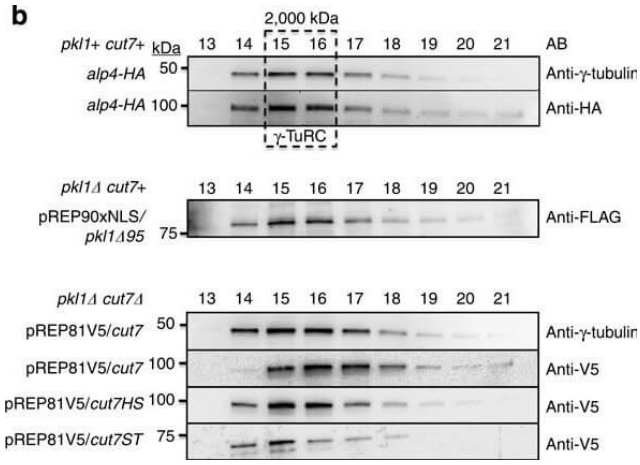

Western Blot

Kinesin-5 Cut7 binds the γ-TuRC MTOC.(a) Kinesin-5 and kinesin-14 constructs used in Fast Protein Liquid Chromatography. V5-tagged Cut7 and two truncation constructs were used, in addition to one FLAG-Pkl1 truncated construct that retains full Pkl1 activity. Cut7 constructs are V5-tagged full-length Cut7 (aa 1–1,085), Cut7-Head-Stalk (Cut7HS, aa 1–888) and Cut7-Stalk-Tail (Cut7-ST, aa 443–1,085). (b) Western blot profiles of whole-cell extracts fractionated by Separose 6 using FPLC. (c) Western blots of Cut7 constructs immunoprecipitated from whole-cell extracts using anti-V5 magnetic beads with empty strain negative controls. (d) Cartoon diagram of 6-His tagged Pkl1 Tail peptide co-immunoprecipitation assay using magnetic beads with His affinity and FPLC fraction 15. (e) Pkl1 Tail peptide co-immunoprecipitation of γ-TuRC core subunits and V5-Cut7ST using a short Pkl1 Tail peptide (PγT). Mutated peptide PγM has significantly reduced interaction with the fission yeast γ-TuRC. The anti-HA antibody detects the HA-tagged γ-TuRC protein Alp4. Figure provided by CiteAb. Source: Nat Commun, PMID: 25348260.

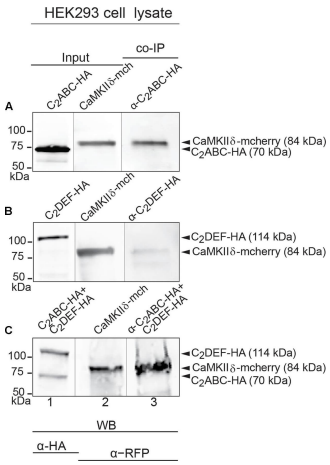

Western Blot

Immunoprecipitation and western blot show interaction of otoferlin with CaMKIIδ. (A–C) Two HA-tagged mouse otoferlin fragments, C2ABC (aa 1–632 in NP_001093865; 70 kDa) and C2DEF (aa 933–1920; 114 kDa) were co-transfected with mcherry-tagged mouse CaMKIIδ into HEK293 cells. Transfections were performed either with otoferlin C2ABC and CaMKIIδ (A, Input Lane 1 and 2), otoferlin C2DEF and CaMKIIδ (B, Input Lane 1 and 2) or in the presence of both C2ABC and C2DEF fragments and CaMKIIδ (C, Input Lane 1 and 2). Co-immunoprecipitations of C2ABC-HA and C2DEF-HA were conducted from HEK293 cell lysates using anti-HA antibodies. CaMKIIδ-mcherry was detected in the eluate using an anti-RFP (red fluorescent protein) antibody (A–C, Lane 3), indicating that CaMKIIδ co-precipitated with recombinant otoferlin fragments. Figure provided by CiteAb. Source: Front Synaptic Neurosci, PMID: 29046633.

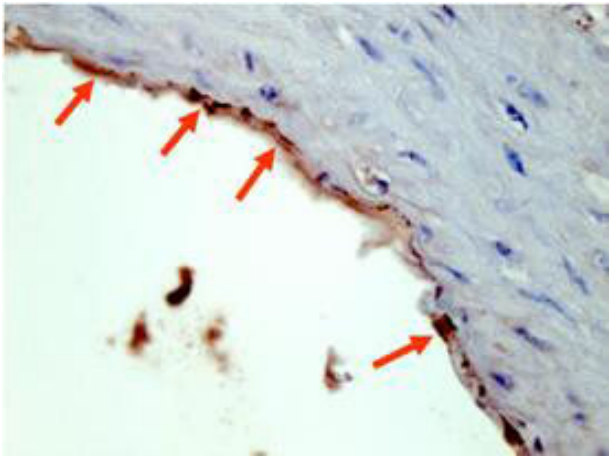

Immunohistochemistry

Rockland's Affinity Purified anti-HA epitope tag polyclonal antibody detects HA tagged recombinant proteins by IHC on formalin fixed paraffin embedded tissue. Arrowheads point to expression of HA tagged proteins in endothelial cells of mouse aorta. Sections of 4 µm were prepared from representative paraffin blocks. Sections were then deparaffinized and rehydrated with xylene and alcohol. Citrate buffer antigen retrieval was performed for 30 min in a boiling jar. Anti-HA was diluted in blocking buffer at 1:2,000 and reacted at 4° C overnight followed by signal detection using horseradish peroxidase with DAB as the chromogenic substrate. Tissue was counterstained with Mayer's hematoxylin. Personal Communication, Behzad Yeganeh,U. Manitoba, Winnipeg, Canada.

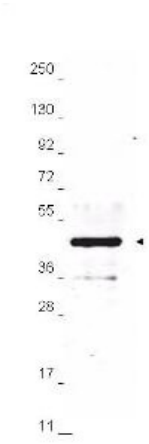

Western Blot
Anti-HA epitope tag polyclonal antibody detects HA-tagged recombinant proteins by western blot. Polyclonal Rabbit anti-HA epitope tag, at a 1:2,000 dilution, was used to detect 1.0 µg of 12-Epitope Tag Protein Marker Lysate (p/n MB-301 -0100) containing the HA epitope tag. A 4-20% gradient gel was used to resolve the protein by SDS-PAGE. The lysate was transferred to nitrocellulose using standard methods. After blocking, the membrane was probed with Rockland's anti-HA tag antibody for 1 h at room temperature followed by washes and reaction with a 1:20,000 dilution of IRDye® 800 conjugated Gt-a-Rabbit IgG (H&L) MX10 (code 611-132-122) for 30 min at room temperature. LICOR's Odyssey® Infrared Imaging System was used to scan and process the image. Other detection systems will yield similar results.

References

- Wang Y et al. TRIM29 promotes bladder cancer invasion by regulating the intermediate filament network and focal adhesion. *Oncogene.* (2025)
- Zhang X et al. Stress granule-localized USP8 potentiates cGAS-mediated type I interferonopathies through deubiquitination of DDX3X. *Cell Rep.* (2024)
- Cheng Z et al. HECTD3 inhibits NLRP3 inflammasome assembly and activation by blocking NLRP3-NEK7 interaction. *Cell Death Dis.* (2024)
- Pickering S et al. Differential dysregulation of β-TrCP1 and -2 by HIV-1 Vpu leads to inhibition of canonical and non-canonical NF-κB pathways in infected cells. *mBio.* (2023)
- Herrera Moro Chao D et al. Hypothalamic astrocytes control systemic glucose metabolism and energy balance. *Cell Metab.* (2022)
- Oh W et al. CtIP Regulates Mitotic Spindle Assembly by Modulating the TPX2-Aurora A Signaling Axis. *Cells.* (2022)
- Vester, SK et al. SpySwitch enables pH- or heat-responsive capture and release for plug-and-display nanoassembly. *Nature Communications* (2022)
- Zajac AL et al. Kinesin-directed secretion of basement membrane proteins to a subdomain of the basolateral surface in Drosophila epithelial cells. *Curr Biol.* (2022)
- Fan Y et al. Cullin 4b Complex Targets IRGM1 to Regulate Intestinal Stem Cell Stemness and Niche. *Cell Death Differ.* (2022)
- Rohde C et al. Ebola Virus Activates IRE1α-Dependent XBP1u Splicing. *Viruses.* (2022)
- Cai B et al. USP5 attenuates NLRP3 inflammasome activation by promoting autophagic degradation of NLRP3. *Autophagy.* (2021)
- Stevens, LM et al. Light-dependent N-end rule-mediated disruption of protein function in Saccharomyces cerevisiae and Drosophila melanogaster. *PloS Genetics* (2021)

- Landry, NM et al. SKI activates the Hippo pathway via LIMD1 to inhibit cardiac fibroblast activation. *Basic Research in Cardiology* (2021)
- Mrowiec K et al. The periphilin 1-like BFAR isoform 3 is highly expressed in transcriptionally silent oocytes and involved in RNA metabolism. *Biochim Biophys Acta Mol Cell Res.* (2021)
- Muroi SI et al. C-Terminal Domain of Aquaporin-5 Is Required to Pass Its Protein Quality Control and Ensure Its Trafficking to Plasma Membrane. *Int J Mol Sci.* (2021)
- Gonclaves-Carneiro D et al. Origin and evolution of the zinc finger antiviral protein. *PLoS Pathog.* (2021)
- Hou J et al. USP18 positively regulates innate antiviral immunity by promoting K63-linked polyubiquitination of MAVS. *Nat Commun.* (2021)
- Ulu A et al. Cdk1 phosphorylation negatively regulates the activity of Net1 towards RhoA during mitosis. *Cell Signal.* (2021)
- Carr HS et al. The PDZ domain protein SYNJ2BP regulates GRK-dependent Sst2A phosphorylation and downstream MAPK signaling. *Endocrinology.* (2021)
- Shi X et al. Genetically engineered cell-derived nanoparticles for targeted breast cancer immunotherapy. *Mol Ther.* (2020)
- Cousomeau J et al. Dopamine D2-Like Receptors Modulate Intrinsic Properties and Synaptic Transmission of Parvalbumin Interneurons in the Mouse Primary Motor Cortex. *eNeuro.* (2020)
- Alvarez-Castelao B et al. The switch-like expression of heme-regulated kinase 1 mediates neuronal proteostasis following proteasome inhibition. *Elife* (2020)
- Hoai NB et al. A Chemogenetic Tool that Enables Functional Neural Circuit Analysis. *Cell Rep.* (2020)
- Pati S et al. Chronic chemogenetic activation of forebrain excitatory neurons in postnatal life evokes long-lasting changes in mood-related behavior. *Elife* (2020)
- Riching AS et al. Suppression of canonical TGF-β signaling enables GATA4 to interact with H3K27me3 demethylase JMJD3 to promote cardiomyogenesis. *J Mol Cell Cardiol.* (2020)
- May JP. et al. The Multifunctional Long-Distance Movement Protein of Pea Enation Mosaic Virus 2 Protects Viral and Host Transcripts from Nonsense-Mediated Decay. *mBio* (2020)
- Woods BL. et al. Interplay of septin amphipathic helices in sensing membrane-curvature and filament bundling. *bioRxiv* (2020)
- Stedden CG et al. Planar-polarized semaphorin-5c and plexin A promote the collective migration of epithelial cells in Drosophila. *Curr Biol.* (2019)
- Rohde C et al. Marburg virus regulates the IRE1/XBP1-dependent unfolded protein response to ensure efficient viral replication. *Emerg Microbes Infect.* (2019)
- Bohn JA et al. Flexibility in nucleic acid binding is central to APOBEC3H antiviral activity. *J Virol.* (2019)
- Nuwer JL et al. Anterograde trafficking signals in GABAA subunits are required for functional expression. *Channels (Austin).* (2019)
- Pati S et al. Chemogenetic activation of excitatory neurons alters hippocampal neurotransmission in a Dose-Dependent manner. *eNeuro.* (2019)

- Olsen C et al. Regulation of somatostatin receptor 2 trafficking by C-tail motifs and the retromer. *Endocrinology.* (2019)
- Arakaki AKS et al. The α-arrestin ARRDC3 suppresses breast carcinoma invasion by regulating G protein–coupled receptor lysosomal sorting and signaling. *J Biol Chem.* (2018)
- Kostas M et al. Protein Tyrosine Phosphatase Receptor Type G (PTPRG) Controls Fibroblast Growth Factor Receptor (FGFR) 1 Activity and Influences Sensitivity to FGFR Kinase Inhibitors. *Mol Cell Proteomics.* (2018)
- Yamada T et al. Mitochondrial stasis reveals p62-mediated ubiquitination in Parkin-independent mitophagy and mitigates nonalcoholic fatty liver disease. *Cell Metab.* (2018)
- Ulu et al. Stress-activated MAPKs and CRM1 regulate the subcellular localization of Net1A to control cell motility and invasion. *Journal of Cell Science* (2018)
- Kijima et al. HSP90 inhibitors disrupt a transient HSP90-HSF1 interaction and identify a noncanonical model of HSP90-mediated HSF1 regulation. *Scientific Reports* (2018)
- Yue et al. SARS-Coronavirus Open Reading Frame-3a drives multimodal necrotic cell death. *Cell Death & Disease* (2018)
- Lv et al. S. pombe Uba1-Ubc15 Structure Reveals a Novel Regulatory Mechanism of Ubiquitin E2 Activity. *Molecular Cell* (2017)
- Kanter et al. A Novel Mechanism for the Grid-to-Place Cell Transformation Revealed by Transgenic Depolarization of Medial Entorhinal Cortex Layer II. *Neuron* (2017)
- Blanco-Melo et al. Co-option of an endogenous retrovirus envelope for host defense in hominid ancestors. *Elife* (2017)
- Bohn et al. APOBEC3H structure reveals an unusual mechanism of interaction with duplex RNA. *Nature Communications* (2017)
- Meese et al. Activity-Dependent Phosphorylation by CaMKIIδ Alters the Ca2+ Affinity of the Multi-C2-Domain Protein Otoferlin. *Frontiers in Synaptic Neuroscience* (2017)
- Yoshii T et al. Pharmacogenetic reactivation of the original engram evokes an extinguished fear memory. *Neuropharmacology.* (2017)
- Kim MW et al. Time-gated detection of protein-protein interactions with transcriptional readout. *Elife* (2017)
- Wu et al. Potassium and the K+/H+ Exchanger Kha1p Promote Binding of Copper to ApoFet3p Multi-copper Ferroxidase. *Journal of Biological Chemistry* (2016)
- Smith et al. Cadmium and Secondary Structure-dependent Function of a Degron in the Pca1p Cadmium Exporter. *Journal of Biological Chemistry* (2016)
- Smith et al. Endoplasmic Reticulum-associated Degradation of Pca1p, a Polytopic Protein, via Interaction with the Proteasome at the Membrane. *Journal of Biological Chemistry* (2016)
- York et al. The RNA Binding Specificity of Human APOBEC3 Proteins Resembles That of HIV-1 Nucleocapsid. *PLOS Pathogens* (2016)
- Pitoniak et al. Cdc42p-interacting protein Bem4p regulates the filamentous-growth mitogen-activated protein kinase pathway. *Molecular and Cellular Biology* (2015)
- Vink et al. Impact of Adenovirus E4-ORF3 Oligomerization and Protein Localization on Cellular Gene Expression. *Viruses* (2015)

- Zhu et al. Gain-of-function p53 mutants co-opt chromatin pathways to drive cancer growth. *Nature* (2015)
- Puighermanal E et al. drd2-cre:ribotag mouse line unravels the possible diversity of dopamine d2 receptor-expressing cells of the dorsal mouse hippocampus. *Hippocampus.* (2015)
- Wei W et al. YCF1-mediated cadmium resistance in yeast is dependent on copper metabolism and antioxidant enzymes. *Antioxid Redox Signal.* (2014)
- MacVicar TDB et al. Impaired OMA1-dependent cleavage of OPA1 and reduced DRP1 fission activity combine to prevent mitophagy in cells that are dependent on oxidative phosphorylation. *J Cell Sci.* (2014)
- Olmsted ZT et al. Kinesin-14 and kinesin-5 antagonistically regulate microtubule nucleation by γ-TuRC in yeast and human cells. *Nat Commun.* (2014)
- Kutluay SB et al. Global changes in the RNA binding specificity of HIV-1 gag regulate virion genesis. *Cell.* (2014)
- Oh W et al. Rho gtpase independent regulation of atm activation and cell survival by the rhogef net1a *Cell Cycle* (2014)
- Freschi L et al. qPCA: a scalable assay to measure the perturbation of protein–protein interactions in living cells. *Mol Biosyst.* (2013)
- Olmsted ZT et al. Kinesin-14 Pkl1 targets γ-tubulin for release from the γ-tubulin ring complex (γ-TuRC). *Cell Cycle.* (2013)
- Jiang S et al. Starch-binding domain-containing protein 1 (Stbd1) and glycogen metabolism: Identification of the Atg8 family interacting motif (AIM) in Stbd1 required for interaction with GABARAPL1. *Biochem Biophys Res Commun.* (2011)
- Niederkofler V et al. Nectin-like molecules/SynCAMs are required for post-crossing commissural axon guidance. *Development.* (2010)
- Chen PY et al. FRS2 via fibroblast growth factor receptor 1 is required for platelet-derived growth factor receptor beta-mediated regulation of vascular smooth muscle marker gene expression. *J Biol Chem.* (2009)

Disclaimer